Planet. Space Sci., Vol. 36, No. 1, pp. 89–97, 1988
Printed in Great Britain.

0032-0633/88 $3.00 + 0.00

NON-THERMAL DISTRIBUTION OF O(^{1}D) ATOMS IN THE NIGHT-TIME THERMOSPHERE*

JENG-HWA YEE
Space Physics Research Laboratory, Univeristy of Michigan, Ann Arbor, MI 48109, U.S.A.

(*Received in final form* 3 *September* 1987)

Abstract—The 6300 Å O(^{1}D–^{3}P) emission has been used for many years to remotely monitor the thermospheric temperature from the Doppler width of its line profile. The O(^{1}D) atoms in the night-time thermosphere are initially produced by the dissociative recombination of O_2^+ ions with kinetic energy much greater than the thermal energy of the ambient neutrals. The validity of the technique to monitor neutral ambient temperature by measuring O(^{1}D) 6300 Å emission depends on the degree of thermalization of the O(^{1}D) atoms. The object of this study is to calculate the velocity distribution of the O(^{1}D) atoms and to examine the effect of non-thermal distribution on the night-time thermospheric neutral temperature determined.

1. INTRODUCTION

The metastable O(^{1}D) atoms give rise to the well-known 6300 Å red line emission in the airglow spectra. Aeronomers have been using this emission line for many years to remotely monitor the thermospheric temperature and neutral wind from the Doppler width and shift of its line profile (Biondi and Feibelman, 1968; Hays and Roble, 1971; Thuillier *et al.*, 1977; Hernandez, 1980, 1982; Biondi and Meriwether, 1985). The O(^{1}D) atoms in the night-time thermosphere are initially produced by the dissociative recombination of O_2^+ ions with kinetic energy much greater than the thermal energy of the ambient neutrals. Whether the O(^{1}D) 6300 Å emission can be used to monitor neutral temperature depends on the degree of thermalization of the O(^{1}D) atoms, that is, on whether the energy and momentum distributions of the O(^{1}D) atoms after many collisions with the ambients would represent the characteristics of the ambient neutrals.

It has been known for some time that the optically determined neutral temperatures are consistently higher than those predicted by models or obtained by incoherent radar measurements. Hays *et al.* (1970) made a comparison between radar and optical temperature measurements in the *F*-region and found that their measured mean Doppler temperature was systematically higher than the backscatter temperature by ~45 K, which was within the claimed accuracy limits. Hernandez (1982) analyzed the Doppler temperature values obtained at midlatitudes (Fritz Peak Observatory, Colorado) from 1972 to 1979 and found that his measured values exceed the MSIS model predictions (Hedin *et al.*, 1977; Hedin, 1983) by an average of 100 ~ 150 K. More recently, Biondi and Meriwether (1985) reported a difference of ~180 K between the MSIS model and their measurements obtained at a station in Arequipa, Peru. They discounted the non-thermal broadening effect and suggested that part of the MSIS temperature data base deduced from the *in situ* mass spectrometer measurements may be low and subsequently giving a lower neutral temperature prediction.

The degree of thermalization of the O(^{1}D) atoms depends upon three factors: the collision frequency with the ambient particles, the chemical lifetime, and the velocity distribution with which the O(^{1}D) atoms are initially produced. Biondi and Feibelman (1968) first looked into the possibility of non-thermal O(^{1}D) energy distribution both theoretically and experimentally and concluded that there was no evidence for or against a dissociative origin of the O(^{1}D) atoms from the measured 6300 Å line profiles. The O(^{1}D) atom has a very long radiative lifetime, ~110 s (Garstang, 1951; Froese-Fischer and Saha, 1983). Biondi and Feibelman attributed their conclusion to the possible rapid thermalization of O(^{1}D) atoms before radiation can occur. In the region between 200 and 300 km where the O(^{1}D) atoms are mostly produced (Biondi and Feibelman, 1968; Hays *et al.*, 1978), the main ambient neutral species are ground state O(^{3}P) atoms and N_2 with densities in the order of 10^9 cm^{-3}. One would expect that any newly created energetic O(^{1}D) atoms would suffer tens to hundreds of collisions and become thermalized before they radiate.

In fact, it is believed that collisions with the ambient

* Dedicated to ALEX DALGARNO in his sixtieth year in honour of his many important contributions to aeronomy.

$O(^3P)$ atoms are mostly responsible for the $O(^1D)$ thermalization. Because of molecular symmetry, an excited atom and a normal atom of the same kind may interact in either of two ways. The two atoms may exchange their identities with no transfer of momentum or energy in an excitation energy exchange collision or they may simply be elastically scattered (Mott and Massey, 1965). The excitation transfer collision is a very effective thermalization process for the newly created energetic $O(^1D)$ atoms (Biondi and Feibelman, 1968; Schmitt *et al.*, 1981). As Biondi and Feibelman (1968) stated, only if such a resonant excitation transfer cross-section is small, will fast $O(^1D)$ atoms radiate before losing their excitation to slow $O(^3P)$ atoms in the *F*-region.

Recently, Yee and Dalgarno (1987) using scattering theory calculated the cross-sections for both excitation transfer and elastic scattering which occur in an $O(^1D)$–$O(^3P)$ collision. They found the excitation transfer cross-section to be 6.3×10^{-16} cm^2, only 1/4 of the total collision cross-section. Their results gave a smaller $O(^1D)$ thermalization cross-section than expected, but consistent with the laboratory recombination studies involving excited states of neon and argon (Connor and Biondi, 1965; Frommhold and Biondi, 1966).

The chemical lifetime also influences the degree of $O(^1D)$ thermalization. Quenching by ambient species such as N_2 can compete with radiation, and its rate coefficient has been experimentally determined to be 2.3×10^{-11} cm^3 s^{-1} at the temperatures near the *F*-region (Davison *et al.*, 1976; Streit *et al.*, 1976). Recently, by noting the existence of an avoided crossing between the $1^3\Pi_g$ and $2^3\Pi_g$ O_2 molecular states, Yee *et al.* (1985) suggested that quenching by ground state $O(^3P)$ atoms with a calculated rate coefficient of 8.0×10^{-12} cm^3 s^{-1} cannot be ignored in the $O(^1D)$ chemistry. This is substantiated by the analysis of 6300 Å photometric data obtained by the Visible Airglow Experiment on board the *Atmosphere Explorer* satellites (Abreu *et al.*, 1986). The inclusion of $O(^3P)$ quenching provides an additional competition to radiative emission. As a result, the newly created energetic $O(^1D)$ atoms will have less time to become collisionally thermalized.

Although the non-thermal broadening effect has always been believed to be unimportant and ignored in the past, with our newly obtained knowledge of the $O(^1D)$ thermalization cross-sections and chemical loss mechanisms, we are able to re-examine this important question. Here, we theoretically study the velocity distribution of $O(^1D)$ atoms and examine the impact of possible non-thermal broadening on the optical neutral temperature measurements.

2. THEORETICAL MODELS

The main source of $O(^1D)$ atoms at night is the dissociative recombination of O_2^+ ions (Biondi and Feibelman, 1968; Hays *et al.*, 1978; Schmitt *et al.*, 1981) according to the reaction,

$$O_2^+ + e \rightarrow (O_2^*)_{\text{unstable}} \rightarrow \begin{matrix} O^*(^1D) + O^*(^1S) + E_1 \\ O^*(^1D) + O^*(^1D) + E_2 \\ O^*(^1D) + O^*(^3P) + E_3. \end{matrix} \quad (1)$$

This reaction is exothermic, and the excess energy released from the dissociation E_1, E_2 and E_3 would appear as translational energy of the dissociative fragments relative to the center of mass of the parent molecule (as denoted by *). If the O_2^+ ions are in their ground vibrational level, then $E_1 = 0.83$ eV, $E_2 = 3.1$ eV, and $E_3 = 5.0$ eV.

The fate of $O(^1D)$ atoms with supra-thermal kinetic energies depends upon the nature of the interactions following their creation. They may either lose their energies gradually or be chemically quenched through collisions with the ambient thermal gases. Because $O(^1D)$ atoms have a long radiative lifetime, at altitudes greater than 400 km the transport process can be very important (Schmitt *et al.*, 1981). Complete analysis of the $O(^1D)$ energy or velocity distribution as a function of altitude becomes very complicated and involves the coupling of both continuity and diffusion equations. The $O(^1D)$ atoms, however, are mostly produced at altitudes between 200 and 300 km, and collisional thermalization, quenching and radiative emission are still the dominant processes which determine the steady-state velocity distribution. Here we will start with a very simple model to estimate the degree of thermalization of the $O(^1D)$ atoms and examine the possible impact on the temperature determination.

2.1. *Two-population model*

This simple two-population model was first developed by Hays and Walker (1966). The model consists of one subpopulation which is non-thermal and arises from the dissociative recombination of O_2^+. Sinks for the subpopulation include collisional quenching, radiative emission and "thermalization" by ambient N_2 and $O(^3P)$. The second subpopulation is thermally distributed and consists of $O(^1D)$ atoms thermalized by the ambients. Sinks for the thermal subpopulation include collisional quenching and radiation. The two subpopulations are coupled by the "thermalization cross-section" or "thermalization rate" which determines the loss and production in the non-thermal and thermal populations, respectively.

Assuming that the transport of O(^{1}D) is not important, the number densities of the thermal (cold) and non-thermal (hot) populations N_c and N_h can be estimated by solving their continuity equations simultaneously,

$$N_h = \frac{P}{A_{1_D} + (k_{N_2} + K_{N_2})[N_2] + (k_O + K_O)[O]} \quad (2)$$

$$N_c = \frac{K_{N_2}[N_2] + K_O[O]}{A_{1_D} + k_{N_2}[N_2] + k_O[O]} N_h \quad (3)$$

where P is the production rate of non-thermal O(^{1}D) atoms, K_{N_2} and K_O are the thermalization rates by collisions with N_2 and O, k_{N_2} and k_O are the quenching coefficients, and A_{1_D} is the Einstein transition probability of O(^{1}D) atoms. The fraction of the non-thermal population can then be calculated as

$$R = \frac{N_h}{N_h + N_c} = \frac{A_{1_D} + k_{N_2}[N_2] + k_O[O]}{A_{1_D} + (k_{N_2} + K_{N_2})[N_2] + (k_O + K_O)[O]}. \quad (4)$$

The above equation indicates that the fraction of non-thermal population, R, increases with altitude and approaches unity at very high altitudes. This will not happen, however, because the transport process becomes important at such altitudes and the present analysis scheme is no longer valid. At low altitudes where molecular nitrogen is the dominant ambient species, $[N_2] \gg [O]$, and $k_{N_2}[N_2] \gg A_{1_D}$, R is independent of the ambient number density, i.e.

$$R = \frac{k_{N_2}}{k_{N_2} + K_{N_2}}. \quad (5)$$

If we use the measured N_2 quenching rate of 2.3×10^{-11} cm^3 s^{-1} (Streit *et al.*, 1976; Link *et al.*, 1981) and a collisional thermalization rate K_{N_2} ($= \sigma v$, where σ is the thermalization cross-section) $\sim 5 \times 10^{-10}$ cm^3 s^{-1}, R is approximately 4%. It implies that no matter how large the ambient number density gets, the fraction of the non-thermal population will not fall below 4% because of the shorter chemical lifetime. Consider the O(^{1}D) atoms of the non-thermal subpopulation that have an energy of 2.0 eV (average energy acquired from channel 2 and channel 3 of the reaction 1). The average energy of O(^{1}D) atoms (thermal+non-thermal) can therefore be estimated as

$$E_{avg} = (1 - R)^* E_{th} + R^*(2.0 \text{ eV}) \quad (6)$$

where $E_{th} = 3/2kT \sim 1.3 \times 10^{-4}\ T$ eV is the average thermal energy of the ambient neutrals at temperature T. For a temperature of 800 K, the ratio of E_{avg} to E_{th} can be as high as 1.7 and decreases with increasing temperature.

The presence of a non-negligible amount of non-thermal O(^{1}D) atoms will result in a non-Gaussian 6300 Å emission line profile and an error in the temperature determination. The two-population model is very useful to estimate the degree of thermalization of thermospheric O(^{1}D) atoms, or any other species in the atmosphere which might be non-thermal. To examine the magnitude of the temperature error, however, we need to know the shape of the emission line more precisely and the O(^{1}D) distribution to higher energy or velocity resolution.

2.2. *Continuous relaxation model*

The continuous relaxation model has been widely used to calculate the energy distribution of warm atoms in the Earth's atmosphere (Whipple *et al.*, 1975; Logan and McElroy, 1977; Schizgal and Lindenfeld, 1979; Yee and Killeen, 1986). Whipple *et al.* (1975) first developed the model from the kinetic theory of warm atoms to study the non-Maxwellian velocity distributions and resulting Doppler-broadened O(^{1}S) 5577 Å emission line profiles. In treating the warm O(^{1}S) atoms thermalization collisions with ground state O(^{3}P) atoms, they pointed out the possible deficiency in the single relaxation model of Hays and Walker (1966) and investigated the relative importance of both elastic and excitation exchange collisions. Because of the lack of knowledge on the magnitudes of the two cross-sections, no definite answer was given.

Recently, Yee and Dalgarno (1985) calculated the elastic and excitation exchange cross-sections of O(^{1}S)–O(^{3}P) collisions using scattering theory. Using a formula given by Yee and Dalgarno (1985) to treat the collision process numerically, Yee and Killeen (1986) developed a model very similar to the one of Whipple *et al.* to theoretically calculate the energy distribution of the O(^{1}S) atoms in the night-time thermosphere. The model was used to analyze the high spectral resolution line profiles of 5577 Å emision measured by the Fabry–Perot interferometer on board the *Dynamic Explorer* satellite (Hays *et al.*, 1981). They were able to successfully identify the active channel for the O(^{1}S) production and concluded that the main contributor to its production is the dissociative recombination of O_2^+ ions in vibrational levels $v = 1$ and 2, in good agreement with the quantal calculations of Guberman (1983) and the O_2^+ vibrational distribution calculation of Fox (1986).

For the energy distribution of O(^{1}D) atoms at altitudes between 200 and 400 km, if we neglected the transport process, the model is still adequate with only

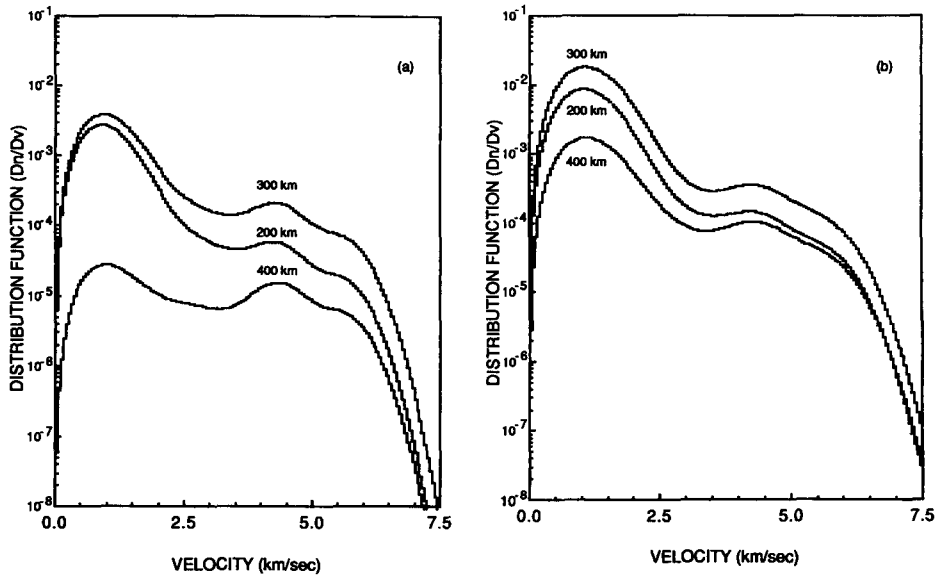

FIG. 1. CALCULATED VELOCITY DISTRIBUTIONS OF THE O(^{1}D) ATOMS AT 200, 300 AND 400 km FOR (a) LOW DENSITY MODEL AND (b) HIGH DENSITY MODEL.

minor modification to include the quenching by N_2 and O(^{3}P) atoms. The cross-sections of elastic scattering and excitation transfer in collisions of O(^{1}D) and O(^{3}P) atoms can be obtained from the calculated results of Yee and Dalgarno (1987).

Similar to the formulations given in Yee and Killeen (1986), the number density of O(^{1}D) atoms N_i having energy between E_i and $E_i+\mathrm{d}E$ can be obtained by solving a series of coupled linear equations,

$$N_i\left\{\sum_{j\neq i}(\alpha_{ij}[O]+\beta_{ij}[N_2])+k_O[O]+k_{N_2}[N_2]+A_{^1D}\right\} = \sum_{n=1}^{3} f_n P_n(E_i)+\sum_{j\neq i} N_j(\alpha_{ji}[O]+\beta_{ji}[N_2]), \quad (7)$$

where α_{ij} is the rate coefficient for the production of an O(^{1}D) atom with energy E_j in the collision of an O(^{1}D) atom with energy E_i and ground state O(^{3}P) atoms with a thermalized energy distribution characterized by a temperature T, and can be calculated by the integral given in equation (8) of Yee and Killeen (1986). β_{ij} is the rate coefficient for the case of elastic collision with molecular nitrogen. $P_n(E_i)$ is the chemical production rate of O(^{1}D) atoms at energy between E_i and $E_i+\mathrm{d}E$ and can be calculated by using equation (4) of Yee and Killeen (1986) for each production channel n with a branching ratio of f_n.

Observations of the 6300 Å red line emission include the contributions from different altitudes along the line of sight. Figure 1 shows the calculated velocity distributions of the O(^{1}D) atoms at several altitudes based upon two model atmospheres described in Table 1. Model I represents an atmosphere which has relatively lower N_2 and O densities. Since the magnitude of the emission shift is proportional to the component of the O(^{1}D) velocity along the line of sight, we have modified the formulations of Yee and Killeen (1986) to work in velocity space. The parameters such as quenching rate coefficients and collision cross-sections are listed in Table 2. The theoretically calculated $A_{^1D}$ coefficient by Froese-Fischer and Saha (1983) is adopted here (Abreu *et al.*, 1986). The branching f_n of the channels leading to the production of O(^{1}D) atoms are not well known. The values selected in this study are given in Table 2, and we will discuss this selection in a later section.

The results show that even at 200 km, the O(^{1}D) atoms are still not completely thermalized just as the two-population model suggests, and become more non-thermal as the altitude increases. Figure 2 shows the comparison between the calculated velocity distribution and the thermalized distribution at 200 km. Because of less thermalization collisions, the O(^{1}D) atoms under low density Model I condition depart more from complete thermalization.

Figure 3 presents the normalized 6300 Å emission line profiles for the velocity distribution under the low density atmospheric condition of Model I assuming that the O(^{1}D) atoms have an isotropic angular distribution. No line-of-sight integration has been performed, and we have considered the emission to be produced in a single layer, i.e. 200, 250 or 300 km,

TABLE 1a. MODEL I (LOW DENSITY) ATMOSPHERIC PARAMETERS

Alt. (km)	n(O)†	$n(N_2)$†	$n(O_2^+)$†	n(e)†	Temp. (K)	η(6300 Å)‡
200.0	1.95(9)§	2.70(9)	2.64(4)	8.00(3)	743.9	2.19(0)
220.0	1.17(9)	1.16(9)	1.01(4)	2.34(4)	764.5	4.61(0)
240.0	7.22(8)	5.13(8)	4.00(3)	5.92(4)	777.0	7.75(0)
260.0	4.56(8)	2.33(8)	1.63(3)	1.30(5)	783.7	1.01(1)
280.0	2.89(8)	1.07(8)	6.69(2)	1.55(5)	788.7	6.45(0)
300.0	1.85(8)	4.95(7)	2.78(2)	1.73(5)	791.9	3.53(0)
320.0	1.20(8)	2.32(7)	1.17(2)	1.80(5)	793.4	1.70(0)
340.0	7.78(7)	1.09(7)	4.93(1)	1.75(5)	794.5	7.43(−1)
360.0	5.06(7)	5.17(6)	2.09(1)	1.70(5)	795.2	3.17(−1)
380.0	3.31(7)	2.47(6)	9.01(0)	1.53(5)	795.6	1.25(−1)
400.0	2.17(7)	1.18(6)	3.88(0)	1.37(5)	795.9	4.91(−2)
420.0	1.43(7)	5.68(5)	1.68(0)	1.23(5)	796.0	1.92(−2)
440.0	9.42(6)	2.74(5)	7.32(−1)	1.10(5)	796.1	7.51(−3)
460.0	6.23(6)	1.33(5)	3.20(−1)	9.80(4)	796.1	2.94(−3)
480.0	4.13(6)	6.48(4)	1.41(−1)	8.37(4)	796.2	1.11(−3)
500.0	2.74(6)	3.16(4)	6.19(−2)	7.14(4)	796.3	4.16(−4)

† Number density in units of cm^{-3}.
‡ Volume emission rate in units of photons $\cdot cm^{-3} \cdot s^{-1}$.
§ 1.95(9) reads 1.95×10^9.

TABLE 1b. MODEL II (HIGH DENSITY) ATMOSPHERIC PARAMETERS

Alt. (km)	n(O)†	$n(N_2)$†	$n(O_2^+)$†	n(e)†	Temp. (K)	η(6300 Å)‡
200.0	5.71(9)	4.17(9)	2.73(4)	5.53(4)	973.0	7.47(0)
220.0	3.83(9)	2.18(9)	1.31(4)	1.06(5)	1000.0	1.12(1)
240.0	2.62(9)	1.16(9)	6.40(3)	1.91(5)	1018.7	1.54(1)
260.0	1.82(9)	6.33(8)	3.19(3)	3.22(5)	1030.3	1.92(1)
280.0	1.29(9)	3.50(8)	1.63(3)	4.48(5)	1035.5	1.89(1)
300.0	9.16(8)	1.95(8)	8.32(2)	5.74(5)	1039.0	1.62(1)
320.0	6.56(8)	1.09(8)	4.29(2)	6.85(5)	1041.3	1.24(1)
340.0	4.72(8)	6.14(7)	2.23(2)	7.84(5)	1042.3	8.68(0)
360.0	3.40(8)	3.47(7)	1.16(2)	8.38(5)	1043.1	5.48(0)
380.0	2.46(8)	1.97(7)	6.09(1)	8.38(5)	1043.5	3.15(0)
400.0	1.78(8)	1.12(7)	3.20(1)	8.25(5)	1043.8	1.74(0)
420.0	1.29(8)	6.43(6)	1.69(1)	8.11(5)	1043.9	9.47(−1)
440.0	9.41(7)	3.69(6)	8.96(0)	7.85(5)	1043.9	5.02(−1)
460.0	6.88(7)	2.13(6)	4.77(0)	7.37(5)	1044.0	2.57(−1)
480.0	5.03(7)	1.23(6)	2.57(0)	6.72(5)	1044.0	1.28(−1)
500.0	3.68(7)	7.12(5)	1.38(0)	6.09(5)	1044.0	6.34(−2)

† Number density in units of cm^{-3}.
‡ Volume emission rate in units of photons $\cdot cm^{-3} \cdot s^{-1}$.

TABLE 2. OTHER PARAMETERS USED IN THE CALCULATION

Branching ratios:	
$f_1 = 0.05$	
$f_2 = 0.4$	(see text)
$f_3 = 0.4$	
Rate coefficients:	
$A_{^1D} = 0.0093\ s^{-1}$	(Froese-Fischer and Saha, 1983)
$k_O = 8.0 \times 10^{-12}\ cm^3\ s^{-1}$	(Yee *et al.*, 1985; Abreu *et al.*, 1986)
$K_{N_2} = 2.3 \times 10^{-11}\ cm^3\ s^{-1}$	(Streit *et al.*, 1976; Link *et al.*, 1981)
Collision cross-sections:	
$\sigma_{el}(O): 1.6 \times 10^{-15}\ cm^2$	(Yee and Dalgarno, 1987)
$\sigma_{ex}(O): 6.7 \times 10^{-16}\ cm^2$	(Yee and Dalgarno, 1987)
$\sigma_{el}(N_2): 3.0 \times 10^{-15}\ cm^2$	(Logan and McElroy, 1977)

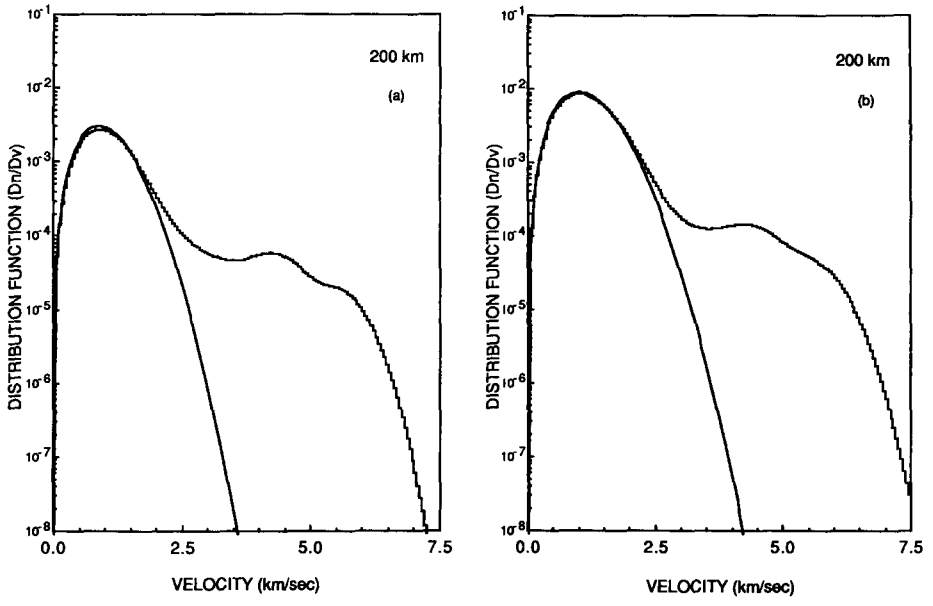

FIG. 2. COMPARISON BETWEEN THE CALCULATED VELOCITY DISTRIBUTION AND THE THERMALIZED DISTRIBUTION OF THE O(^{1}D) ATOMS AT 200 km FOR (a) LOW DENSITY MODEL AND $T = 743.9$ K, AND (b) HIGH DENSITY MODEL AND $T = 973.0$ K.

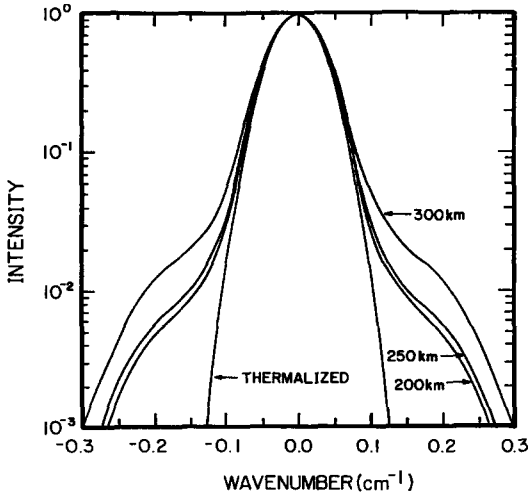

FIG. 3. NORMALIZED 6300 Å VOLUME EMISSION LINE PROFILES AT 200, 250 AND 300 km FOR THE LOW DENSITY MODEL.

respectively. The thermalized emission profile corresponding to a temperature of 743.9 K is also shown for comparison. As we can clearly see, the calculated emission profiles are non-thermal and broadened near the wings. The non-thermal characteristics may not be observable, only a few percent deviation from the thermalization profile, and becomes more apparent as the emission altitude increases. It implies that the error in the deduced temperature from the line-of-sight 6300 Å emission profile can be as much as a few percent and increases as the altitude of the maximum emission increases. The exact magnitude of the error depends upon the instrumental set-up and the temperature deduction technique used in the data analysis.

3. ANALYSIS OF 6300 Å LINESHAPE

High resolution Fabry–Perot interferometers have been widely used to measure 6300 Å emission line profiles. As it was demonstrated, the degree of broadening in the non-thermal 6300 Å emission profile may only be a few percent. Detection of the non-thermal characteristics and the temperature enhancement introduced by the small deviation from a thermalized Gaussian would therefore depend upon the temperature analysis technique. Several analysis techniques, varying from a direct nonlinear least-squares Gaussian fit (Hays and Roble, 1971) to a least-square deconvolution method (Hernandez, 1986), have been adopted for data analysis. Here we use a quasi-linear least-squares fitting method developed for the multichannel Fabry–Perot interferometer on board the *Dynamic Explorer* spacecraft (Killeen and Hays, 1984).

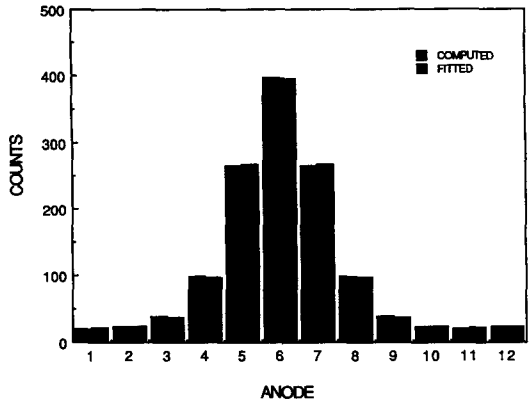

FIG. 4. THE *DE*-FPI SPECTROGRAM SIMULATED FOR A 250 km LINE-OF-SIGHT TANGENT HEIGHT MEASUREMENT FOR THE LOW DENSITY MODEL IN COMPARISON WITH THE SPECTROGRAM BASED UPON A THERMALIZED GAUSSIAN LINE PROFILE OF 867.1 K. The integration period is assumed to be 1 s and the satellite was at 450 km.

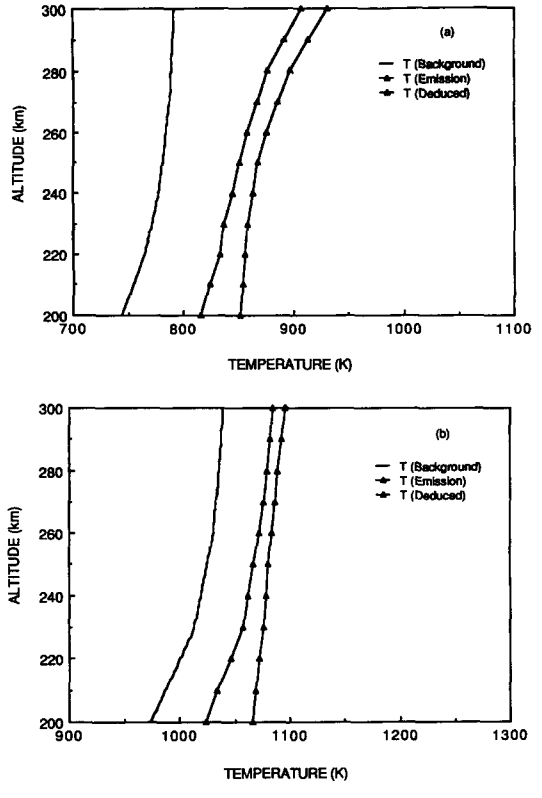

FIG. 5. DEDUCED TEMPERATURE FROM THE COMPUTED LINE-OF-SIGHT SIGNAL AT VARIOUS TANGENT HEIGHTS (▲), THE EMISSION TEMPERATURE (△), TOGETHER WITH THE AMBIENT BACKGROUND TEMPERATURE FOR (a) LOW DENSITY MODEL, AND (b) HIGH DENSITY MODEL.

The FPI output signal is a convolution of the source function and the instrument transfer function. A full description of the Fabry–Perot (*DE*-FPI) instrument on board *Dynamic Explorer*-2 satellite has been given by Hays *et al.* (1981). Figure 4 gives the *DE*-FPI 12 channel spectrograms simulated for low density Model I assuming a satellite altitude of 450 km and a line-of-sight tangent height of 250 km. The temperature from this computed signal is deduced to be 867.1 K, which is about 90 K higher than the ambient temperature. The signal for the fitted Gaussian line profile is also shown in Fig. 4 for comparison.

Figures 5a and 5b present the deduced temperatures from the computed line-of-sight signal at various tangent heights (▲) along with the ambient background gas temperatures, under the atmospheric conditions of Model I and Model II, respectively. The emission temperature (△), the temperature deduced from the volume emission line profile at a given altitude, is also shown in the figure. Due to higher thermalization collision frequency, the deduced temperature is closer to the ambient background temperature as the tangent height gets lower and its difference is smaller, ~50 K for a 250 km tangent height measurement for the high density Model II. Because most of the emission signal is coming from ~260 km (see volume emission rates given in Table 1), the temperature deduced from the intensity measurement at a tangent height of 200 km mainly represents the emission temperature near 260 km (shown by △). This explains why the difference between the deduced temperature and the background temperature appears to become larger as the tangent height gets below 260 km. Another important feature indicated in this figure is that even at very low altitudes where collisions are very frequent, the difference between the emission temperature and the background temperature remains the same. As the altitude decreases, not only does the thermalization collision frequency increase, but the chemical rate is also enhanced. As a result, the O(¹D) atoms have a short chemical lifetime, and the newly created non-thermal O(¹D) atoms would suffer less thermalization collisions before they radiate. This is consistent with what the simple two-population model has previously suggested. No matter how high the ambient density gets, the steady-state velocity distribution of the O(¹D) atoms or the corresponding emission temperature does not vary very much.

4. DISCUSSION

In this paper we have calculated the velocity distribution of the O(¹D) atoms in the night-time ther-

mosphere and examined the degree of departure from the thermalized Gaussian distribution. Some parameters used in our calculation, such as the branching ratios of the source reactions which determine the initial $O(^1D)$ velocity distribution, are not well known. Our results here therefore only represent an estimate. Based upon the branching ratio of 0.9 for the total production of $O(^1D)$ atoms obtained by the laboratory measurements of Zipf (1970), Rohrbaugh and Nisbet (1973) gave a set probabilities of occurrence f_n of 0.05, 0.275 and 0.30 for the three channels, respectively. There are 21 molecular singlet states and 18 triplet states that lead to $O(^1D)$ atoms via the dissociative recombination of O_2^+ (Guberman, 1983). The lowest accessible singlet state which is expected to have large electronic matrix elements and dissociates to two $O(^1D)$ atom is $1\,^1\Delta_u$. It intersects the large R turning point of $v = 0$ and is believed to contribute the most to the $O(^1D)$ production in the $O(^1D)$–$O(^1D)$ channel. The lower accessible triplet state which dissociates to $O(^1D)$–$O(^3P)$ is $1\,^3\Sigma_u^-$. This state is expected to have a large dissociative recombination cross-section for $v = 1$ of $O_2^+(X\,^2\Pi_g)$. Considering the vibrational distribution of O_2^+ and the larger statistical weight for the triplet state, we expect that the dissociative recombination will have a similar probability of occurrence via these two routes. A value of 1.3 for the total branching ratio has been deduced from recent aeronomical studies (Hays *et al.*, 1978; Link *et al.*, 1981; Abreu *et al.*, 1986). We therefore selected the values of f_n to be 0.05, 0.4 and 0.4, respectively, as shown in Table 2. The purpose of this paper is to demonstrate the possible non-thermal $O(^1D)$ distribution and its impact on the optical neutral temperature measurements using the 6300 Å emission line shape. We believe that unless there is little production via the triplet route or the high exothermicity channel $[O_2^+ + e \rightarrow O(^1D) + O(^3P) + 5.0\,eV]$, our analysis here is still valid, and we are currently examining the sensitivity of our results to the various values of f_n.

It can be seen in Fig. 4 that the computed signal can still be fitted very well with a Gaussian, except that a higher temperature is deduced. Consequently, it is extremely difficult to detect any non-thermal signature such as the broadened wings, from the 6300 Å line profile observed from the ground. Any possible non-thermal effects will only be reflected in the deduced temperature. It should be noted here that no detector noise has been added in our analysis, so that the temperature enhancement determined in our study would only appear as a systematic difference. This can explain the systematic enhancement of optically determind temperatures over the MSIS model temperatures (Hernandez, 1982). There are other concerns over the difference of optically determined temperatures and the temperatures determined by Incoherent Scatter (IS) radar measurements (Roble *et al.*, 1968; Hays *et al.*, 1970; Hernandez *et al.*, 1975). This is beyond the scope of our study although it is assumed that at the emission altitudes the ion or electron temperature at night is equal to the neutral temperature. The variation of the peak altitude of the $O(^1D)$ emission layer and the possible large temperature gradient in the region may all contribute to the difference. This has been the subject of the recent paper by McCormac *et al.* (1987). We believe that for our purpose the comparison should be made with the *in situ* measurements by the mass spectrometer such as NATE on board *Atmosphere Explorer* (*AE*) satellites (Spencer *et al.*, 1973) or WATS on board the *Dynamic Explorer* (*DE*) satellite (Spencer *et al.*, 1981), and with the empirical model temperature of MSIS (Hedin, 1983) in which part of the data base was based upon the mass spectrometer data.

Another important process which has been neglected in our study is the transport of $O(^1D)$ atoms to higher altitudes. This has been examined and studied by Schmitt *et al.* (1981) both theoretically and experimentally by using the photometric data obtained from the Visible Airglow Experiment (VAE) on board the *AE* satellite. They showed that in general the transport effect only becomes important above 500 km. They did not, however, explicitly solve the velocity distribution of $O(^1D)$ atoms as a function of altitude. We believe that our analysis may be valid below 400 km, and at higher altitudes, the pure collisional relaxation model will definitely over-estimate the degree of non-thermal distribution since most of the $O(^1D)$ atoms there are transported from the lower altitudes. To accurately obtain the velocity distribution at all altitudes, a model which couples both the continuity equation, the one considered here, and the momentum transport equation should be used. Because the emission rate above 400 km is very small, we believe that the effect of the transport process on the results of our temperature analysis is very small, at least for the ones on the low tangent height measurements.

Acknowledgements—This research was initiated while the author was at Harvard-Smithsonian Center for Astrophysics, working with Prof. Alex Dalgarno. The author wishes to acknowledge the constant support and encouragement of Prof. Dalgarno through the years. Without his guidance, this study would not have been possible. This research was supported at the University of Michigan in part by the NASA grant NAGW-496.

REFERENCES

Abreu, V. J., Yee, J. H., Solomon, S. C. and Dalgarno, A. (1986) The quenching rate of O(^{1}D) by O(^{3}P). *Planet. Space Sci.* **34**, 1143.

Biondi, M. A. and Feibelman, W. A. (1968) Twilight and nightglow spectral line shapes of oxygen λ6300 and λ5577 radiation. *Planet. Space Sci.* **16**, 431.

Biondi, M. A. and Meriwether, J. W., Jr. (1985) Measured response of the equatorial thermospheric temperature to geomagnetic activity and solar flux changes. *Geophys. Res. Lett.* **12**, 267.

Conner, T. R. and Biondi, M. A. (1965) Dissociative recombination in neon: spectral line-shape studies. *Phys. Res. A* **140**, 778.

Davidson, J. A., Sakowski, C. M., Schiff, H. I., Streit, G. E., Howard, C. J., Hennings, D. A. and Schmeltekopf, A. L. (1976) Absolute rate constant determinations for the deactivation of O(^{1}D) by time resolved decay of O(^{1}D) → O(^{3}P) emission. *J. chem. Phys.* **64**, 57.

Fox, J. L. (1986) The vibrational distribution of O_2^+ in the dayside ionosphere. *Planet. Space Sci.* **34**, 1241.

Froese-Fischer, C. and Saha, H. P. (1983) Multi-configuration Hartree–Fock results with Breit–Pauli corrections for forbidden transitions in the 2p4 configuration. *Phys. Res. A* **28**, 3169.

Frommhold, L. and Biondi, M. A. (1966) Dissociative recombination in neon and argon. *Bull. Am. Phys. Soc.* **11**, 493.

Garstang, R. H. (1951) Energy levels and transition probabilities in p2 and p4 configurations. *Mon. Not. R. astr. Soc.* **111**, 115.

Guberman, S. L. (1983) Potential energy curves for the dissociative recombination, in *Physics of Ion–Ion and Electron–Ion collisions* (Edited by Brouillard, F. and McGowan, J. W.), pp. 167–200. Plenum Press, New York.

Hays, P. B., Killeen, T. L. and Kennedy, B. C. (1981) The Fabry–Perot interferometer on *Dynamic Explorer*. *Space Sci. Instum.* **5**, 393.

Hays, P. B., Nagy, A. F. and McWatters, K. D. (1970) Comparison of radar and optical temperature measurements in the *F*-region. *J. geophys. Res.* **75**, 4881.

Hays, P. B. and Roble, R. G. (1971) A technique for recovering Doppler line profiles from Fabry–Perot interferometer fringes of very low intensity. *Appl. Optics* **10**, 193.

Hays, P. B., Rusch, D. W., Roble, R. G. and Walker, J. C. G. (1978) The OI(6300 Å) airglow. *Rev. Geophys.* **16**, 225.

Hays, P. B. and Walker, J. C. G. (1966) Doppler profiles of the 5577 Å airglow. *Planet. Space Sci.* **14**, 1331.

Hedin, A. E. (1983) A revised thermospheric model based on mass spectrometer and incoherent scatter data: MSIS-83. *J. geophys. Res.* **88**, 10170.

Hedin, A. E., Salah, J. E., Evans, J. V., Reber, G. P., Newton, G. P., Spencer, N. W., Kayser, D. C., Alcayde, D., Bauer, P., Cogger, L. L. and McClure, J. P. (1977) A global thermospheric model based on mass spectrometer and incoherent scatter data: MSIS 1. N2 density and temperature. *J. geophys. Res.* **82**, 2139.

Hernandez, G. (1980) Measurement of thermospheric temperatures and winds by remote Fabry–Perot spectrometry. *Opt. Eng.* **19**, 518.

Hernandez, G. (1982) Midlatitude thermospheric neutral kinetic temperatures 1. Solar, geomagnetic and long-term effects. *J. geophys. Res.* **87**, 1623.

Hernandez, G. (1986) *Fabry–Perot Interferometer*. Cambridge University Press, Cambridge, U.K.

Hernandez, G., Van Zandt, T. E., Peterson, V. L. and Turtle, J. P. (1975) Comparison of optical and incoherent scatter measurements of night-time exospheric temperatures at the magnetic equator. *J. geophys. Res.* **80**, 3271.

Killeen, T. L. and Hays, P. B. (1984) Doppler line profile analysis for a multichannel Fabry–Perot interferometer. *Appl. Optics* **23**, 612.

Link, R., McConnell, J. C. and Shepherd, G. G. (1981) A self-consistent evaluation of the rate constants for the production of the OI(6300 Å) airglow. *Planet. Space Sci.* **29**, 589.

Logan, J. A. and McElroy, M. B. (1977) Distribution functions for energetic oxygen atoms in the Earth's lower atmosphere. *Planet. Space Sci.* **25**, 117.

McCormac, F. G., Killeen, T. L. and Nardi, B. (1987) How close are ground-based Fabry–Perot thermospheric wind and temperature measurements to exospheric values? A simulation study. *Planet. Space Sci.* **35**, 1255.

Mott, N. F. and Massey, H. S. W. (1965) *The Theory of Atomic Collisions* (3rd ed.). Oxford University Press, Oxford, U.K.

Roble, R. G., Hays, P. B. and Nagy, A. F. (1968) Calculated [OI] 6300 Å nightglow Doppler temperatures for solar cycle minimum. *Planet. Space Sci.* **16**, 1109.

Rohrbaugh, R. P. and Nisbet, S. N. (1973) Effect of energetic oxygen atoms on neutral density models. *J. geophys. Res.* **78**, 6768.

Schizgal, B. and Lindenfeld, M. J. (1979) Energy distribution function of translationally hot O(^{3}P) atoms in the atmosphere of Earth. *Planet. Space Sci.* **27**, 1321.

Schmitt, G. A., Abreu, V. J. and Hays, P. B. (1981) Nonthermal O(^{1}D) produced by dissociative recombination of O_2^+: a theoretical model and observational results. *Planet. Space Sci.* **29**, 1095.

Spencer, N. W., Niemann, H. B. and Carignan, G. R. (1973) The neutral-atmosphere temperature instrument. *Radio Sci.* **8**, 284.

Spencer, N. W., Wharton, L. E., Niemann, H. B. and Hedin, A. E. (1981) The *Dynamic Explorer* wind and temperature spectrometer. *Space Sci. Instrum.* **5**, 417.

Streit, G. E., Howard, C. J., Schmeltekopf, A. L., Davison, J. A. and Schiff, H. I. (1976) Temperature dependence of O(^{1}D) rate constants for reactions with O_2, N_2, CO_2, O_3 and H_2O. *J. chem. Phys.* **65**, 4761.

Thuillier, G., Galin, J. L. and Wachtel, C. (1977) Experimental global model of the exospheric temperature based on measurements from the Fabry–Perot interferometer on board the *OGO*-6 satellite—discussion of the data and properties of the model. *J. atmos. terr. Phys.* **39**, 399.

Whipple, E. C., Jr., Van Zandt, T. E. and Love, C. H. (1975) Kinetic theory of warm atoms: non-Maxwellian velocity distributions and resulting Doppler-broaden emission line profiles. *J. chem. Phys.* **62**, 3204.

Yee, J. H. and Dalgarno, A. (1985) Energy transfer of O(^{1}S) atoms in collisions with O(^{3}P) atoms. *Planet. Space Sci.* **33**, 825.

Yee, J. H. and Dalgarno, A. (1987) Energy transfer of O(^{1}D) atoms in collisions with O(^{3}P) atoms. *Planet. Space Sci.* **35**, 399.

Yee, J. H., Dalgarno, A. and Guberman, S. (1985) Quenching of O(^{1}D) atoms by collisions with O(^{3}P) atoms. *EOS Trans.* **66**, 993.

Yee, J. H. and Killeen, T. (1986) Thermospheric production of O(^{1}S) atoms by dissociative recombination of vibrationally excited O_2^+. *Planet. Space Sci.* **34**, 1101.

Zipf, E. C. (1970) The dissociative recombination of O_2^+ ions into specifically identified final atomic states. *Bull. Am. Phys. Soc.* **15**, 418.